ce/papers Proceedings in civil engineering

Ernst & Sohn A Wiley Brand

ORIGINAL ARTICLE

eurosteel AMSTERDAM 2023

Ernst & Sohn A Wiley Brand

Effect of heat treatment on microstructure and pseudoelasticity of a memory-steel

Maryam Mohri[1] | Christian Leinenbach[1,2] | Dimitrios G. Lignos[3] |Elyas Ghafoori[1,4]

Correspondence

Dr. Maryam Mohri
Empa, Swiss Federal Laboratories for Materials Science and Technology
Uberlandstrasse 129
8600 Dübendorf
Email: maryam.mohri@empa.ch

[1] Empa, Swiss Federal Laboratories for Materials Science and Technology, Dübendorf, Switzerland
[2] Laboratory for Photonic Materials and Characterization, École Polytechnique Fédérale de Lausanne (EPFL), Lausanne, Switzerland
[3] Civil Engineering Institute, École Polytechnique Fédérale de Lausanne (EPFL), Lausanne, Switzerland
[4] Institute for Steel Construction, Faculty of Civil Engineering and Geodetic Science, Leibniz University Hannover, Hannover, Germany

Abstract

The pseudoelasticity behavior of memory-steels has recently gained attention for applications in seismic-resistant structures. The pseudoelasticity can be used to reduce residual deformations in building structures subjected to seismic loading. Fe-based shape memory alloys (Fe-SMA), which is also called as memory-steel, have gained much attention because of their strong shape memory behavior and low material manufacturing cost, which justify their large-scale application in construction. This research investigated the effects of heat treatment on microstructure and pseudoelasticity of a memory-steel (Fe-17Mn-5Si-10Cr-4Ni-1(V,C) %wt.). Various solution-annealing treatments from 1000 to 1200 °C for 2 h and aging from 650, 750 and 850 °C were applied to investigate the microstructural evolution and pseudoelasticity behavior of the alloy. The results showed that increasing the solution annealing temperature caused grain growth and pseudoelasticity loss. On the other hand, the precipitation of (Cr,V)Cs after aging resulted in an improved pseudoelasticity. The large elastic strain field, which forms near the carbide precipitates, improves the pseudoelasticity. Furthermore, precipitates can provide preferential nucleation sites for the martensite phase and a high density of stacking faults in the austenite matrix. The study concludes that the best pseudoelasticity behavior was achieved after an aging at 750°C for 6 h.

Keywords

Intelligent metal, memory steel, Fe-based shape memory alloy, Superelasticity, Heat treatment, Microstructure.

1 Introduction

Memory-steels, which is also known as Fe–Mn–Si-based shape memory alloys (SMAs), have gained a significant research interest as one of the most practical types of Fe-based SMAs for civil engineering applications [1-2]. These alloys have been widely used in various applications such as coupling devices, structural elements, pre-stressing of structures, and damping devices due to their low material cost, high Young's modulus and strength, exceptional workability, and high stress recovery [3-4]. However, their limited pseudoelasticity (PE) has hindered their use in applications like dissipative re-centring systems in civil engineering. A new Fe-Mn-Si-based SMA composition, Fe–17Mn–5Si–10Cr–4Ni–1(V,C), containing nano-sized VC, has been developed with potential applications in civil engineering [5-6]. The alloy was designed and optimized to have a rather strong shape memory effect suitable for pre-stressed strengthening of civil structures [6]. The microstructural cause of the PE effect in Fe-Mn-Si-based SMAs is thought to be a blend of Shockley partial dislocations that move in reverse and the back transformation from ε-martensite (which has a hexagonal close-packed (hcp) lattice structure) to γ-austenite (which has a face-centred cubic (fcc) lattice structure) during unloading. To enhance the PE of Fe-Mn-Si-based SMAs, various efforts have been made, including controlling grain size and texture, and precipitation, in conjunction with controlling stacking fault energy (SFE) [7-9].

Studies have shown that the strength of the γ phase can be increased by the presence of carbide precipitates, which aid in the reversible movement of the γ/ε interfaces along a specific crystallographic pathway. This back transformation is brought about by the back-stress on the growing ε-martensite lath resulting from the stress fields generated by the carbides [10]. Additionally, precipitates help form martensite by decreasing the critical resolved shear stress of austenite. Precipitates also raise the number of dislocations and stacking faults in the γ matrix, which serve as embryos for ε nucleation [11]. Recently, it has been discovered that fine-grained austenite matrix

https://doi.org/10.1002/cepa.2734 wileyonlinelibrary.com/journal/cepa

with a uniformly dispersed array of precipitates facilitates the γ ⇌ ε transformation and enhances the PE properties of the alloy [12,13].

There has been limited research conducted on how to improve the PE behaviour of Fe-Mn-Si-based SMAs. Consequently, there is a requirement for further studies to gain a deeper understanding of the PE mechanisms present in these alloys. The objective of this investigation is to examine, how solution annealing and aging treatment can affect the PE of the Fe–17Mn–5Si–10Cr–4Ni–1(V, C) alloy.

2 Experimental procedure

2.1 Outline and formal structure

In this study, a Fe-based SMA supplied by re-fer AG in a shape of strip that was produced through induction melting in air followed by hot rolling. The chemical composition of the alloy was Fe–17Mn–5Si–10Cr–4Ni-1(V, C) (%wt.). Electrical discharge machining (EDM) was used to create dog-bone-shaped specimens from strips that had a thickness of 1.5 mm. The dimensions and shape of the dog-bone specimens are displayed in Figure 1.

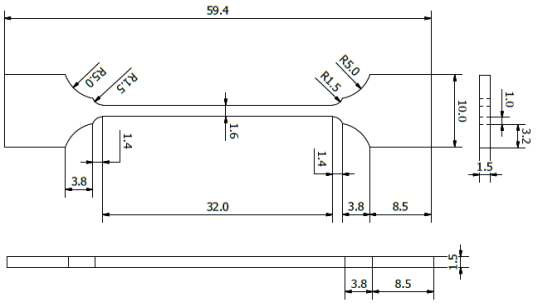

Figure 1 Schematic of the dog-bone-shaped specimen (unit: mm).

The as-received samples were subjected to a heat treatment, which included solution-annealing at 1000, 1100 and 1200 °C for 2 h followed by water quenching. The solution-annealed samples were the aged at from 650, 750 and 850 °C for various dwell times (2,4,6 and 8h), followed by air-cooling. The microstructures of specimens were analysed using scanning electron microscopy (SEM; FEI NanoSEM230), transmission electron microscopy (TEM; FEI Tecnai F20 series).For SEM observation, the samples underwent polishing and were then etched with a solution of H_2O_2 and HNO_3 along with HCl in the ratio of 7:30:9. The TEM specimens, on the other hand, were prepared using standard electro-polishing. Perchloric acid and ethanol (1:9) were used as the electrolytic solution at a temperature of -20°C and voltage of 22 V.

To assess the PE behaviour, quasi-static strain-controlled tensile tests were conducted using a universal tensile testing machine (Z020; Zwick/Roell). The strain evolution was measured with a calibrated sensor-arm extensometer type BTC-EXMULTI.011 with a gauge length of 20 mm. The set-up of tensile test is shown in Fig.2a. The tests were carried out at two different strain levels, 2% and 5%, and a consistent displacement rate of 0.5 mm/min was maintained throughout the experiment.

In this study, the strain that was regained due to PE is referred to as the recovered strain (ε_{pe}). This strain is reversible and occurs during the unloading phase as a result of the transformation of the ε-martensite phase to austenite. The calculation of ε_{pe} was conducted by subtracting the elastic strain (ε_{el}) from the total strain variation that occurred during unloading (ε_{ul}), which can be expressed as follows:

$$\varepsilon_{pe} = \varepsilon_{ul} - \varepsilon_{el} \quad (1)$$

Figure 2 displays schematically a stress-strain curve of the typical Fe-based SMA, along with the relevant definitions.

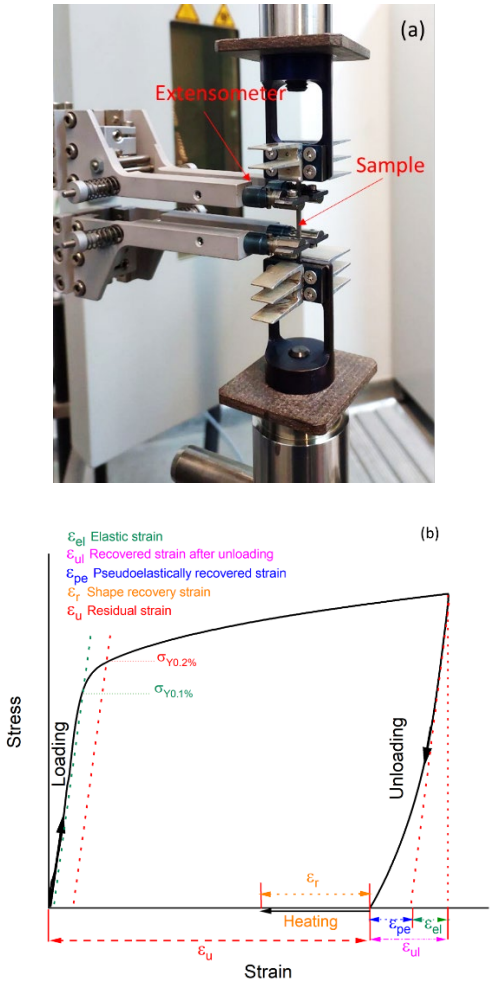

Figure 2 (a) The tensile test setup, (b) Typical stress-strain curve of the Fe-based SMA.

3 Results and discussion

3.1 Mechanical characterization

To analyse the mechanical properties of the samples, cyclic strain-controlled tensile tests at a displacement rate of 0.5 mm/min were conducted. Figure 3 illustrates the stress-strain curves of the solution annealed and aged samples under loading-unloading conditions. A non-linear unloading due to the PE behaviour was oserved. The PE-recovered strain was calculated by applying Eq. (1), and Table 1 displays the values for the material's yield strength ($\sigma_{y0.1\%}$). Previous research indicates that the phase transformation from austenite to martensite occurred at stress levels significantly below $\sigma_{y0.2\%}$ [14-15]. As the limit of

proportionality, $\sigma_{y0.1\%}$, representing 0.1% of the nonlinear strain was taken. Until a yield stress of $\sigma_{y0.1\%}$, the deformation remained elastic. Further deformation was potentially due to the transformation from γ-austenite to ε-martensite (caused by the alloy's low SFE) and dislocation glide. After the $\sigma_{y0.2\%}$ point, dislocation glide and slip played a more substantial role in the deformation. The solution-annealed samples showed a lower yield stress and PE than the as-received sample (Figure 3a). Hence, it is anticipated that solution-annealed samples would exhibit a reduced proportion of martensite and a greater extent of irreversible plastic deformation, resulting in a decrease in PE. The strength and PE of both the as-received and solution-annealed samples were enhanced by the aging treatment as shown in Figure 3b.

The effect of various aging treatments on the mechanical behaviour of as-received samples are displayed in Figure 4. The carbide precipitates that formed in the austenite during aging were responsible for reducing the martensite transformation stress ($\sigma_{y0.1\%}$) and increasing the slip resistance of the matrix ($\sigma_{y0.2\%}$) at room temperature, which led to an increase in the PE of the aged samples. During subsequent loading, the aged samples exhibited a more pronounced strain-hardening behaviour, which is a characteristic of the fcc to hcp transformation. The interaction between different martensite variants and the interplay between the tips of the martensite plates and grain boundaries and carbide resulted in work hardening in the aged samples. The formation of precipitates in the aged specimens resulted in an increase in the yield strength of austenite ($\sigma_{y0.2\%}$) and impeded slip deformation.

Table 1 Description of the different types of furnishing

Specimens	ε_{pe} at 2% strain	ε_{pe} at 5 % strain
AR	0.44 (0%)*	0.74 (0%)*
SA:1000°C	0.21 (-52%)	0.34 (-54%)
SA:1100°C	0.06 (-86%)	0.22 (-70%)
SA:1200°C	0.02 (-95%)	0.12 (-84%)
AR- AG	0.51 (+16%)	0.85 (+15%)
SA:1000°C-AG	0.42 (-4%)	0.73 (-1%)
SA:1100°C-AG	0.34 (-23%)	0.62 (-16%)
SA:1100°C-AG	0.25 (-43%)	---

*The degree of changes compared to the as-received sample, AR: as-received, SA: solution-annealed, AG: aged at 850 °C for 2h.

Figure 4 shows that, as the aging time increased, the $\sigma_{y0.1\%}$ decreased, which indicates that stress induced martensite formation is facilitated and consequently PE is improved. The maximum PE of about 0.62% was observed for the sample aged at 750 °C for 6 h. The different mechanical behaviour of samples aged at various temperature is related to the size and distribution of carbide precipitates in austenitic matrix, which will be discussed in the next section.

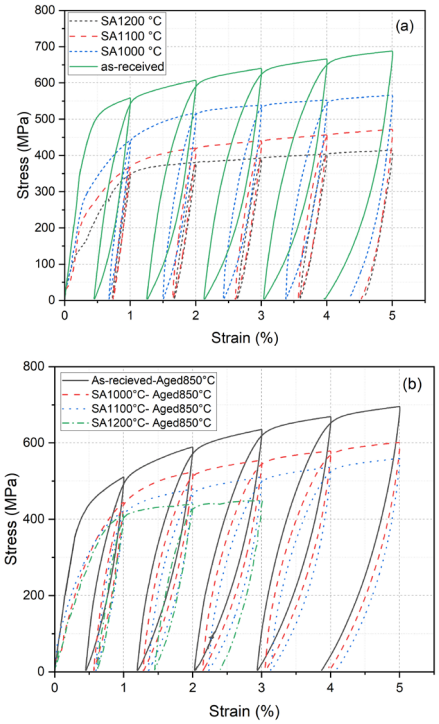

Figure 3 Cyclic stress-strain curve of (a) as-received and solution-annealed samples for 2h, and (b) followed by aging at 850 °C for 2h.

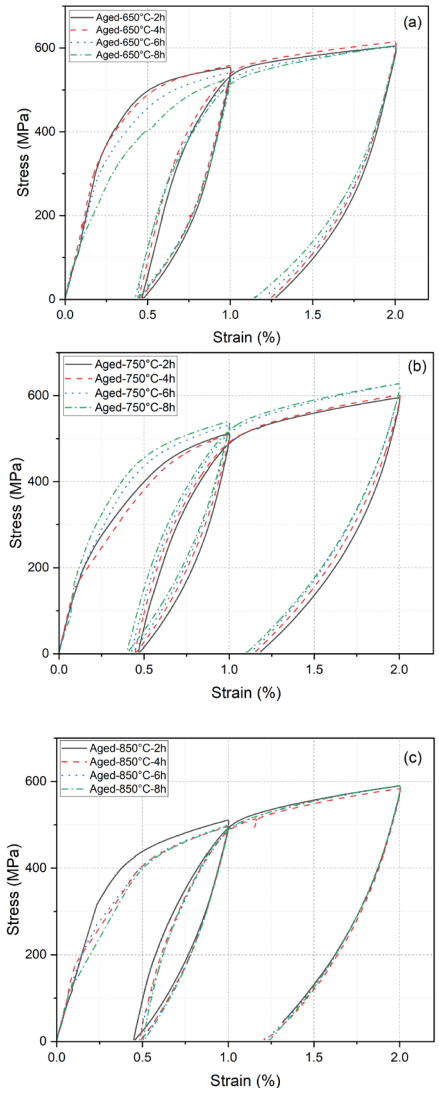

Figure 4 Cyclic stress-strain curve of as-received samples aged at (a) 650 °C, (b) 750 °C, and (c) 850 °C for 2,4,6, and 8h.

3.2 Microstructural characterization

The microstructure's characteristics, following solution annealing and aging, were evaluated using SEM. Figure 5 shows the micrograph of the as-received and solution annealed samples for 2h at 1000 °C, 1100 °C and 1200 °C. According to the data in Figure 5a, it appears that the mean grain size of the as-received sample was around 12 μm, and a few of the grains displayed some precipitates and prominent annealing twins as large bands, which is a common phenomenon in the alloys having low SFE [16]. Furthermore, thin strips, believed to be ε-martensite, were detected in certain grains. It is speculated that the ε-martensite developed during the grinding process. The mean size of the grains grew, following the solution treatment and with increase of annealing temperature, the size of austenite grains has increased sharply. The largest average grain size corresponds to the sample annealed at a temperature of 1200 °C, which is about 600 μm. Furthermore, solution annealing led to the complete dissolution of precipitates in austenitic matrix. The stress-strain graphs presented in Figure 3 indicate an enhanced strength for the as-received specimen, possibly due to the Hall-Petch phenomenon. This effect can be attributed to the smaller grain size of the as-received sample as compared to the solution-annealed samples illustrated in Figure 5. Because of the bigger grain size, the solution-annealed samples exhibited a negligible PE than the as-received samples. The growth grain results in lower austenite stability and PE due to predominance of slip deformation.

Figure 6 compares the microstructure of the samples aged at various temperatures for 6h. At lower temperatures (e.g., 650 °C), fine precipitates were randomly distributed in the austenite matrix due to a higher driving force for precipitation (Figure 6a). During aging treatment at 750 and 850 °C, Cr and/or V carbides with an elongated shape precipitate within the grains and along the boundaries. It can be seen that the average precipitate size has increased with increasing aging temperature. The varying amounts and sizes of precipitates found in the aged samples at temperatures of 650, 750, and 850 °C can be explained by the kinetics of precipitate formation. The process of precipitate formation involves two stages: nucleation and growth, which are significantly affected by the temperature at which aging occurs [7]. When aging occurs at higher temperatures, the nucleation rate is typically lower because the driving force for precipitation is smaller. As a result, there are fewer precipitates with a lower number density. In contrast, interstitial carbon diffuses faster than vanadium. As a result, the growth of VC is limited by vanadium diffusion from the austenite matrix to the precipitate. The diffusion coefficient of vanadium is an exponential function of temperature, and higher temperatures result in larger carbides with fewer numbers and vice versa [17]. Furthermore, longer aging times result in larger precipitates as shown for aged sample at 750 °C for 8h in Fig.6d. The diffusion of alloying elements within the matrix promotes the growth of precipitates.

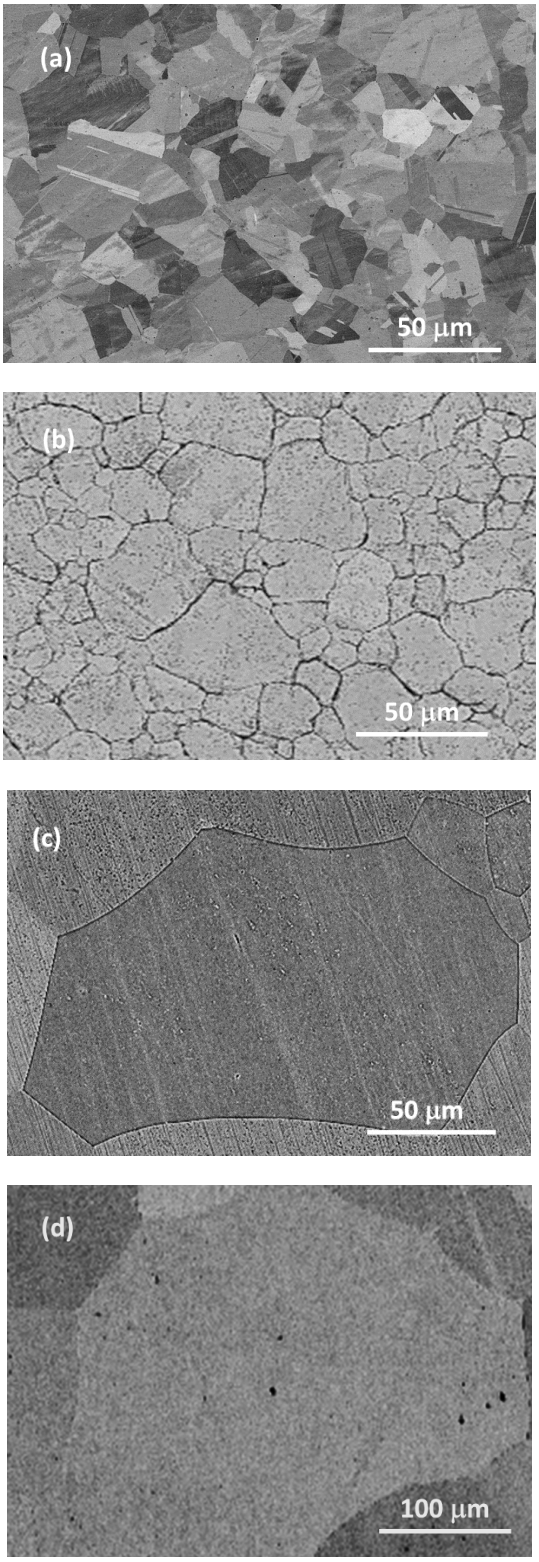

Figure 5 SEM images of (a) as-received, and (b-d) solution-annealed at 1000 °C, 1100 °C, and 1200 °C for 2h, respectively.

The highest PE value was observed in the aged sample when it was kept at 760 °C for 6 hours. Therefore, the microstructure of this sample was analysed using bright field (BF) TEM images along the [100] zone axis. Figure 7 shows stacking faults and nanoscale precipitates. Generally, the precipitates were located near the stacking faults, which were visible as straight lines. Figure 7 shows that the precipitates were present both in the austenite matrix and on the stacking faults. Furthermore, the image dis-

plays visible contrasts of elastic distortion around the precipitates, indicating a state of semi-coherency between the matrix and the precipitates. This semi-coherency creates an elastic strain field surrounding the precipitates, which is believed to act as a spring-back mechanism for the reverse transformation of ε (hcp) to γ (fcc) during unloading [18]. This mechanism leads to an enhancement in the material's PE behaviour. Furthermore, residual stresses in the near of the precipitates increased the ε transformation temperature and served as nucleation sites for the growth of the ε phase.

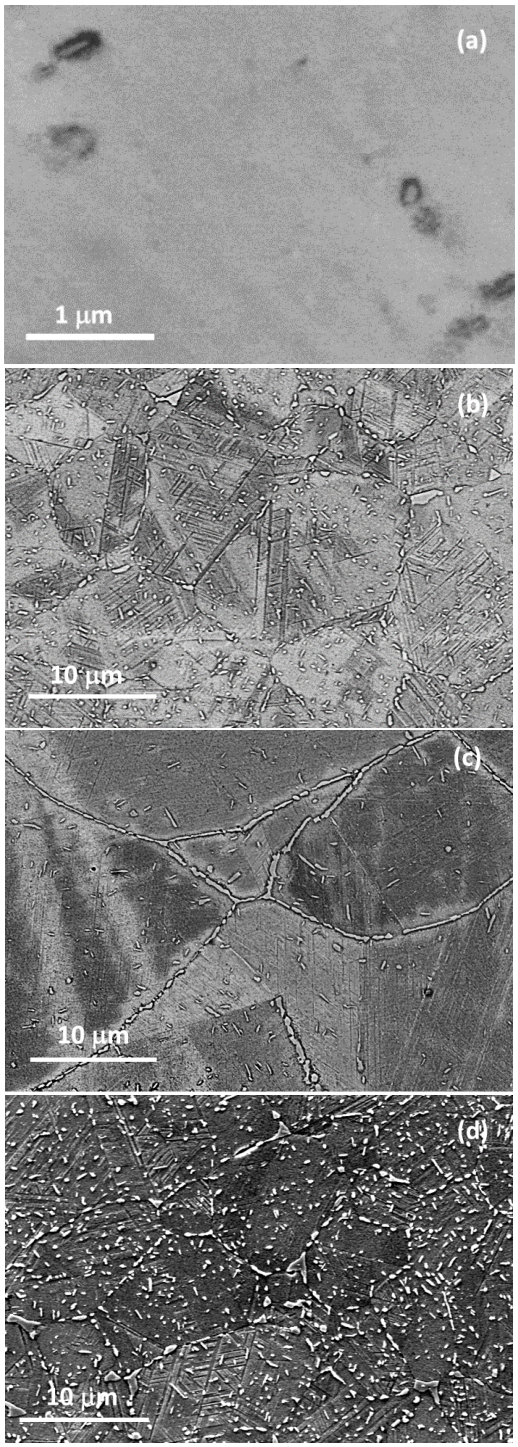

Figure 6 SEM images of as-received samples which aged at (a) 650 °C, (b) 750 °C, (c) 850 °C for 6h, and (d) 750 °C for 8h.

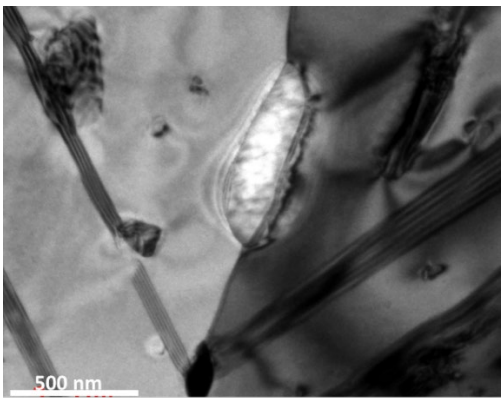

Figure 7 TEM image of aged sample at 750°C for 6h.

4 Conclusion

Although the Fe-based SMA (i.e., the so called memory steel composed of Fe–17Mn–5Si–10Cr–4Ni-1(V, C)) has been found to be suitable as a prestressing component for civil infrastructures, an improvement in the pseudoelastic behaviour of the alloy can make it a potentially interesting alternative to NiTi SMAs for seismic applications in construction. In this study, the influence of heat treatment (solution-annealing and aging) on the microstructure and mechanical properties (PE and yield stress) of the alloy was investigated. The results showed that heat treatments led to a significant improvement in the pseudoelasticity of the memory steel. Based on the experimental results and microstructural evaluations, the following conclusions were drawn:

1. The as-received samples exhibited a higher level of pseudo-elasticity than the solution annealed samples. The superior performance of the as-received specimens can be attributed to their microstructure, which contains smaller grains that impact the interaction between martensite-ε plates and grain boundaries.
2. The formation of carbide precipitates with a uniform distribution during aging resulted in the emergence of stacking faults and ε-martensite in the microstructure. The interaction of these precipitates with the tips of the martensite plates created a spring back stress for reverse transformation (from martensite to austenite), which improved the pseudo-elasticity and also increased work-hardening in the aged samples.
3. The microstructures of the aged samples are strongly influenced by the aging temperature. At lower temperature fine precipitates were randomly distributed in the austenite matrix due to a higher driving force for precipitation. Conversely, at higher temperatures, the significantly greater diffusion rate of the alloying elements and smaller driving force for precipitation in the matrix caused solute atoms to segregate to grain boundaries and resulted in formation of bigger precipitates at these boundaries.

5 Acknowledgments

This study was funded by the EMPAPOSTDOCS-II program, which received funding from the European Union Horizon 2020 research and innovation program under the

Marie Skłodowska-Curie grant agreement number 754364. The contribution of re-fer AG in providing the test materials is also acknowledged. Any opinion and findings in this paper are those of the authors and do not necessarily reflect the view of the sponsors.

References

[1] Vollmer, M.; Segel, C.; Krooß, P.; Günther, J.; Tseng, L. (2015) On the effect of gamma phase formation on the pseudoelastic performance of polycrystalline Fe–Mn–Al–Ni shape memory alloys, Scr Mater. 108, pp.23–26.

[2] Bauer, A.; Vollmer, M.; Niendorf, T. (2021) Effect of Crystallographic Orientation and Grain Boundaries on Martensitic Transformation and Superelastic Response of Oligocrystalline Fe–Mn–Al–Ni Shape Memory Alloys, Shape Memory and Superelasticity. 7, pp.373–382.

[3] Peng, H.; Wang, G.; Wang, S.; Chen, J.; MacLaren, I.; Wen, Y. (2018) Key criterion for achieving giant recovery strains in polycrystalline Fe-Mn-Si based shape memory alloys, Materials Science and Engineering: A. 712, pp.37–49.

[4] Gu, X.L.; Chen, Z.Y.; Q.Yu, Q.; Ghafoori, E. (2021) Stress recovery behavior of an Fe-Mn-Si shape memory alloy, Eng Struct. 243, pp. 112710.

[5] Dong, Z.; Klotz, U.E.; Leinenbach, C.; Bergamini, A.; Czaderski, C.; Motavalli, M. (2009) A novel Fe-Mn-Si shape memory alloy with improved shape recovery properties by VC precipitation, Adv Eng Mater. 11, pp.40–44.

[6] Hosseini, E.; Ghafoori, E.; Leinenbach, C.; Motavalli, M.; Holdsworth, S.R. (2018) Stress recovery and cyclic behaviour of an Fe–Mn–Si shape memory alloy after multiple thermal activation, Smart Mater Struct. 27, pp.025009.

[7] Arabi-Hashemi, A.; Lee, W.J.; Leinenbach, C. (2018) Recovery stress formation in FeMnSi based shape memory alloys: Impact of precipitates, texture and grain size, Mater Des. 139.

[8] Matsumura, O.; Sumi, T.; Tamura, N.; Sakao, K.; Furukawa, T.; Otsuka, H. (2000) Pseudoelasticity in an Fe–28Mn–6Si–5Cr shape memory alloy, Materials Science and Engineering: A. 279, pp. 201–206.

[9] Leinenbach, C.; Arabi-Hashemi, A.; Lee, W.J.; Lis, A.; Sadegh-Ahmadi, M.; van Petegem, S.; Panzner, T.; van Swygenhoven, H. (2017) Characterization of the deformation and phase transformation behavior of VC-free and VC-containing FeMnSi-based shape memory alloys by in situ neutron diffraction, Materials Science and Engineering: A. 703, pp. 314–323.

[10] Khodaverdi, H.; Mohri, M.; Ghafoori, E.; Sabet Ghorabaei, A.; Nili-Ahmadabadi, M.; (2022) Enhanced pseudoelasticity of an Fe–Mn–Si-based shape memory alloy by applying microstructural engineering through recrystallization and precipitation, Journal of Materials Research and Technology. 21C, pp. 2999–3013.

[11] Khodaverdi, H.; Mohri, M.; Ghorabaei, A.S.; Ghafoori, E.; Nili-Ahmadabadi, M. (2023) Effect of low-temperature precipitates on microstructure and pseudoelasticity of an Fe–Mn–Si-based shape memory alloy. Materials Characterization 195, pp. 112486.

[12] Mohri, M.; Ferretto, I.; Leinenbach, C.; Kim, D.; G. Lignos, D.; Ghafoori, E. (2022) Effect of thermomechanical treatment and microstructure on pseudo-elastic behavior of Fe–Mn–Si–Cr–Ni-(V, C) shape memory alloy, Materials Science and Engineering: A. 855, pp. 143917.

[13] Mohri, M.; Ferretto, I.; Leinenbach, H.; Khodaverdi, H.; Ghafoori, E. (2023) influence of thermomechanical treatment on the shape memory effect and pseudoelasticity behavior of conventional and additive manufactured Fe-Mn-Si-Cr-Ni-(V,C) shape memory alloys, Journal of Materials Research and Technology. 24, pp. 5922–5933.

[14] Lee, W.J.; Weber, B.; Feltrin, G.; Czaderski, C.; Motavalli, M.; Leinenbach, C. (2013) Phase transformation behavior under uniaxial deformation of an Fe–Mn–Si–Cr–Ni–VC shape memory alloy. Materials Science and Engineering: A. 581, pp. 1-7.

[15] Koster, M.; Lee, W.J.; Schwarzenberger, M.; Leinenbach, C. (2015) Cyclic deformation and structural fatigue behavior of an FE–Mn–Si shape memory alloy. Materials Science and Engineering: A. 637, pp. 29-39.

[16] Benzing, J.T.; Poling, W.A.; Pierce, D.T.; Bentley, J. ; Findley, K.O.; Raabe, D.; Wittig, J.E. (2018) Effects of strain rate on mechanical properties and deformation behavior of an austenitic Fe-25Mn-3Al-3Si TWIP-TRIP steel. Materials Science and Engineering: A. 711, pp. 78-92.

[17] Maugis, P.; Goune, M. (2005) Kinetics of vanadium carbonitride precipitation in steel: a computer model, Acta Mater. 53, pp. 3359–3367.

[18] Yazawa, Y.; Furuhara, T.; Maki, T. (2004) Effect of matrix recrystallization on morphology, crystallography and coarsening behavior of vanadium carbide in austenite, Acta Mater. 52, pp. 3727–3736.